WARSAW UNIVERSITY OF TECHNOLOGY Index 351733
FACULTY OF CIVIL ENGINEERING
COMMITTEE FOR CIVIL AND WATER ENGINEERING
POLISH ACADEMY OF SCIENCES ISSN 1230-2945
DOI: 10.24425/ace.2024.151914
ARCHIVES OF CIVIL ENGINEERING
Vol. LXX ISSUE 4 2024
pp. 631–647

Research paper

Resistance model for confined circular reinforced concrete columns under eccentric loads

Marta Lutomirska[1], Aleksander Szwed[2], Aneta Krystyna Łuszczyńska[3], Tomasz Andrzej Lutomirski[4]

Abstract: Circular reinforced concrete columns with spiral reinforcement exhibit an increased ductility and resistance due to the confinement effect. Many experimental investigations and theoretical studies related to this topic are focused on columns under axial load, while those for eccentric load are seldom. The scope of the paper is to present a developed calculation model of resistance for eccentrically loaded confined circular concrete columns. The model assumptions extend procedures of the ACI and Eurocode to the confined concrete case. In order to determine the resistance of columns in the form of the force-moment interaction diagrams, a special procedure is elaborated and described in detail. The peak stress and corresponding strain for axially loaded confined concrete is calculated using the Richart's model. Then, an increase of ultimate strength capacity due to confinement is related to the axial strain level. The more the eccentricity, the less the confinement effect is engaged in the column resistance. The contribution of spiral reinforcement in the bearing capacity is the greatest in concentrically loaded columns and it vanishes at the point where axial strain in the concrete column is equal to zero, which initially governed the beneficial effect of the spiral reinforcement. A sample interaction diagram is obtained for the selected design case and compared with the diagram for unconfined column.

Keywords: circular columns, confinement, interaction diagrams, spiral reinforcement, reinforced concrete, resistance model

[1]PhD., Warsaw University of Technology, Faculty of Civil Engineering, Al. Armii Ludowej 16, 00-637 Warsaw, Poland, e-mail: marta.lutomirska@pw.edu.pl, ORCID: 0000-0002-9673-0432
[2]PhD., Warsaw University of Technology, Faculty of Civil Engineering, Al. Armii Ludowej 16, 00-637 Warsaw, Poland, e-mail: aleksander.szwed@pw.edu.pl, ORCID: 0000-0002-7746-8221
[3]MSc., PhD Student, Auburn University, Faculty of Civil and Environmental Engineering, 238 Harbert Center, Auburn, Alabama 36849 , USA, e-mail: akl0091@auburn.edu, ORCID: 0009-0004-2795-2033
[4]PhD., Gaz-System S.A., ul. Jana Kazimierza 578, 05-126 Nieporęt, Rembelszczyzna, Poland, e-mail: lutomirski.tomasz@gmail.com, ORCID: 0000-0001-6527-1045

1. Introduction

Columns are crucial elements responsible for the safety of structures. Initially designed to carry just compressive forces, since reinforced concrete became widespread, they are designed for compression, flexure, and shear. Additionally, they are required to possess adequate ductility, which allows higher deformations without significant loss of resistance in case of earthquakes. Circular spirally reinforced columns respond to these needs, which makes them more popular among structural designers and a valuable object for researchers. Restraint caused by the lateral reinforcement improves both the bearing and deformation capacity of confined concrete columns [1]. However, the lateral confining stress (strain) and the axial compressive stress (strain) are interrelated, and thus not easy to evaluate [2].

For the first time the advantages of confinement for axially loaded circular columns with spiral transverse reinforcement were presented over one hundred years ago by A. Considére [3]. Further contribution was provided by other researchers and a number of models for confined concrete have been developed. F.E. Richart et al. [4] revealed two extremes of resistance, first before loss of concrete cover and second at high longitudinal deformation. An influence of the amount of the transverse reinforcement investigated by A. Kuryłło [5] was found to decrease for higher classes concrete. H. Rüsch, S. Stöckl, and B. Menne [6, 7] led extensive research on the effect of short-term and long-term loading on resistance of spirally reinforced columns. The conclusions turned out to be very sceptical, proving that the effective use of spiral reinforcement is possible just for very high values of long-term loadings, which imply exceedingly high longitudinal strain and the solution becomes impractical for serviceability conditions. A. Nowakowski [8] studied strain in longitudinal and transverse reinforcement for different statical schemas. Studies by T. Godycki-Ćwirko, P. Korzeniowski, K. Nagrodzka-Godycka [9] concluded that the number of spirals significantly influences resistance only for small eccentricities. With increasing eccentricity and concrete strength, the beneficial role of spirals disappears, since strains in transverse reinforcement are several times smaller than in the longitudinal reinforcement. An extensive overview of research related to theory and laboratory tests on columns is presented in a book by P. Korzeniowski [10]. Recent studies focus on many material and structural aspects: their behaviour under seismic or accidental loading, application of different types of concrete, steel grade, layout and type of lateral reinforcement, reinforcement with polymers and shape memory alloys [1, 11–18], and reliability-based design and code calibration [19–27], among others. Studies conducted on the non-circular cross-section proved that the confinement is less effective than in circular columns due to stress concentration at the corners resulting in flat sides without any confining pressure [12, 18, 28].

F.E. Richart et al. [4] became the initiators of the experimentally validated formula representing strength and the corresponding longitudinal strain of confined concrete due to active hydrostatic pressure tested on cylinder specimens. During the experiment, the cylinder samples were subjected to an increasing axial stress, whereas the lateral confining pressure was held constant. The aim of that research was to compare the strength of the concrete resulting from lateral fluid pressure (active confinement) with the strength generated by circular spirals situated close to each other to create an equivalent amount of lateral pressure (passive confinement).

Ultimate compressive strength and corresponding ultimate strain are significantly higher for confined concrete than for unconfined. Confining pressure is caused by the transverse dilation of concrete (owing to Poisson's effect) due to applied axial strain. At the beginning of loading process the magnitude of lateral strain increases steadily with the axial strain. Next at about 70-80% of the peak stress load splitting cracks are formed due to bonding failure, followed by delamination and slip at the aggregate-paste interfaces [2]. Then the magnitude of lateral strain increases much more rapidly with the axial strain. At this stage the confinement effect is active, the unconfined concrete cover spalls off, whereas the concrete core continues to sustain the higher stress at high strains. The effectiveness of confinement relies on many parameters and factors such as compressive strength of concrete, aggregate type, amount of longitudinal, and type and amount of transverse reinforcement [1, 2, 9].

The stress-strain curve of confined concrete has a shallower slope of the descending part. The strength of a spirally reinforced confined column is more dependent on the yield strength of confining reinforcement than compressive strength of concrete [28]. For this reason, the failure occurs due to the fracture of the confining reinforcement. First hoop fracture controls the confined ultimate compressive strength. At initial loading stages concrete is unaffected by the confinement reinforcement.

Deformability of concrete beyond the peak stress strongly depends on longitudinal reinforcement which is susceptible to buckling after the concrete cover spalls off. The stability of longitudinal reinforcement depends on the amount of transverse reinforcement. In summary, there is a need to provide sufficient amount of lateral reinforcement in relation to the unsupported length of longitudinal bars. After fulfilling that condition, the reinforcement cage may provide effective confinement against the lateral expansion of the concrete. The confinement effect improves with higher transverse reinforcement ratio. Nevertheless, it is not realistic to exceed the practical range of the reinforcement ratio beyond the one provided by the codes [29, 30].

A model for confined concrete circular columns under eccentric load proposed by A.M. Abd El Fattah [31] was based on Mander et al. [28]. In the numerical and iterative model, the column cross-section is divided into a finite number of thin layers. For the nonlinear stress-strain relation the force and moment of each layer is calculated and stored and the rebars are treated as discrete objects in their actual locations. The resultant axial force under concentric loading and pure bending moment are calculated, and then by an interpolation function eccentricity is introduced. The results are presented on the interaction diagram. However, it considers much larger involvement of the confinement in the resistance and vanishes at pure bending (infinite eccentricity), which according to the authors and literature [1] overestimates capacity of eccentrically loaded column for increasing bending moment.

Many confinement models for concrete columns under concentric axial loads were proposed over the years and compared to experimental work. They are mostly focused on prediction of the stress-strain curve, whose shape may depend on various material and geometrical parameters. However, the confined column behaviour under eccentric load generating bending moment in addition to axial load remains unresolved satisfactory. Even though there is a small number of laboratory tests on eccentrically loaded spiral columns [12, 18, 31], the force-moment interaction diagrams have not been generated for them.

The scope of this paper is to develop an analytical model that allows presenting resistance of eccentrically loaded confined circular concrete columns in the form of such diagrams. The proposed procedure can be considered as a generalization of procedures used in ACI code [29] and the Eurocode [30]. Thus, software was developed for the calculation of nominal resistance of circular confined concrete columns according to the new eccentricity-based analysis [27]. A detailed procedure of the analysis is described in the paragraphs below. The intended use of this model refers to design and reliability analysis.

2. Model of resistance for confined columns

2.1. General assumptions

A new procedure for determination of nominal cross-sectional resistance of circular concrete columns confined by spiral transverse reinforcement is developed and described in the paragraphs below. The objective of the procedure is to consider not only axial loading, when the confined effect is maximum, but all possible force and moment combinations. The following general assumptions are made in the analysis:

- Richart's model [4] is used for calculation of the maximum (peak) stress and corresponding strain for concentric axially loaded confined concrete.
- A distribution of concrete compressive stress is described as an equivalent rectangular block.
- A perfect bond between the reinforcement steel bars and the concrete is assumed.
- Distribution of strains along the depth of the cross-section is assumed to be linear (plane sections hypothesis).
- Strain compatibility between concrete core and lateral reinforcement.
- A concrete cover can be included into the confined section or completely removed.
- For longitudinal reinforcement the stress-strain relationship is assumed as linear elastic followed by perfectly plastic, for spiral reinforcement the elastic-plastic stress-strain relationship is applicable only to tension.

2.2. Proposed model of confinement effect evaluation

The value of stress in the spiral reinforcement σ_{sL} is described by Eq. (2.1):

$$\sigma_{sL} = \begin{cases} E_{sL} \cdot \varepsilon_{sL} & \text{for } 0 \leq \varepsilon_{sL} \leq \varepsilon_{yL} \\ f_{yL} & \text{for } \varepsilon_{sL} > \varepsilon_{yL} \end{cases} \tag{2.1}$$

where: E_{sL} – modulus of elasticity of spiral reinforcement, ε_{sL} – strain in spiral reinforcement, $\varepsilon_{yL} = f_{yL}/E_{yL}$ – yield strain in spiral reinforcement, f_{yL} – yield stress of spiral reinforcement.

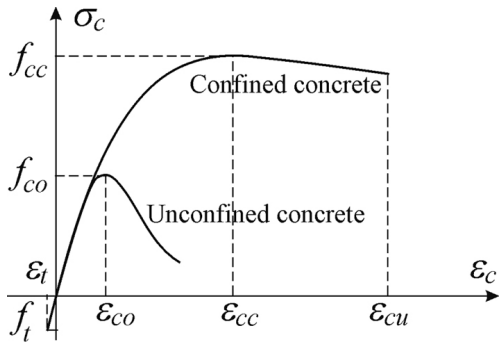

Fig. 1. Stress-strain relationships for unconfined and confined concrete

The confined concrete compressive peak strength f_{cc} and the corresponding strain in confined concrete ε_{cc}, as shown in Fig. 1, are calculated as proposed by F. E. Richart [4], using Eq. (2.2).

$$f_{cc} = f_{co} + k_1 \cdot f_L \varepsilon_{cc} = \varepsilon_{co} \cdot \left(1 + k_2 \cdot \frac{f_L}{f_{co}}\right) \tag{2.2}$$

where: f_{co} – compressive strength of unconfined concrete, k_1 – coefficient assumed to be equal 4.1 (or different value if supported by experiments), f_L – the lateral pressure defined by Eq. (2.3), ε_{co} – compressive strain corresponding to f_{co}, k_2 – coefficient equal to $5k_1$ (or different value if supported by experiments).

The equilibrium of forces, established under the condition that the tension from the transverse steel exerts a uniformly distributed (smeared) lateral pressure f_L on a core of the concrete column, allows determination of the lateral pressure by Eq. (2.3):

$$f_L = \frac{\sigma_{sL} \cdot A_{sL}}{R \cdot s} \tag{2.3}$$

where: A_{sl} – area of spiral reinforcement, R – radius of the concrete column's section, s – spiral pitch.

As recognised in the literature, evaluation of the lateral strain of confined concrete under nonlinear and inelastic condition remains a difficult task. At initial state of loading the value of Poisson's ratio for concrete is about 0.2 and concrete can be treated as a linear isotropic material. During an increase of axial compression, it remains almost constant up to approximately $0.8 f_{co}$, then it starts to grow rapidly up to 0.5 or an even larger value, since due to tensile splitting concrete converts to an orthotropic material. For this reason, at the peak stress the concrete is assumed to be an incompressible isotropic material with value of Poisson ratio equal to 0.5 [2], for which analysis of axially loaded columns leads to the compatibility relationship $\varepsilon_A = 2 \cdot \varepsilon_{sL}$ between the axial strain in a concrete column ε_A and the strain in spiral reinforcement ε_{sL}.

Under bending moment load one half of a column's cross-section is in tension and another half is in compression, then the resultant of accompanying lateral expansion or contraction of a column almost cancel. Thus, only the axial strain results in an increase of column's perimeter,

which causes the confinement effect. This conclusion is valid for symmetric materials in a tension-compression response and symmetric section of a column, while for nonsymmetric materials it is fulfilled approximately, what is the case in the following derivations. Therefore, using strain compatibility it is possible to relate the longitudinal axial strain to the lateral pressure in the defined strain ranges by Eq. (2.4). Consequently Eq. (2.2) for the maximum confined concrete stress and the corresponding strain may be transformed, so the effect of confinement f_{cc} is related to the axial strain ε_A with associated strain ε_{cc}, as described by Eq. (2.5) and Eq. (2.6). Coefficient k_3 introduced in Eq. (2.7) depends on the material model constants, reinforcement, and column geometry.

$$f_L = \begin{cases} \frac{f_{yL} \cdot A_{sL}}{R \cdot s} \cdot \left(\frac{\varepsilon_A}{2 \cdot \varepsilon_{yL}} \right) & \text{for } 0 \le \varepsilon_A \le 2 \cdot \varepsilon_{yL} \\ \frac{f_{yL} \cdot A_{sL}}{R \cdot s} & \text{for } \varepsilon_A > 2 \cdot \varepsilon_{yL} \end{cases} \tag{2.4}$$

$$f_{cc} = f_{co} + k_1 \cdot f_L = \begin{cases} f_{co} + k_1 \cdot \frac{f_{yL} \cdot A_{sL}}{R \cdot s} \cdot \left(\frac{\varepsilon_A}{2 \varepsilon_{yL}} \right) & \text{for } 0 \le \varepsilon_A \le 2 \cdot \varepsilon_{yL} \\ f_{co} + k_1 \cdot \frac{f_{yL} \cdot A_{sL}}{R \cdot s} & \text{for } \varepsilon_A > 2 \cdot \varepsilon_{yL} \end{cases} \tag{2.5}$$

$$\varepsilon_{cc} = \varepsilon_{co} \cdot \left(1 + k_2 \frac{f_L}{f_{co}} \right) = \begin{cases} \varepsilon_{co} \cdot \left(1 + k_3 \cdot \frac{\varepsilon_A}{2 \varepsilon_{yL}} \right) & \text{for } 0 \le \varepsilon_A \le 2 \cdot \varepsilon_{yL} \\ \varepsilon_{co} \cdot (1 + k_3) & \text{for } \varepsilon_A > 2 \cdot \varepsilon_{yL} \end{cases} \tag{2.6}$$

$$k_3 = k_2 \cdot \frac{f_{yL} \cdot A_{sL}}{f_{co} \cdot R \cdot s} \tag{2.7}$$

Therefore, the maximum stress in confined concrete $f_{cc\mathrm{MAX}}$ and corresponding maximum strain $\varepsilon_{cc\mathrm{MAX}}$, which are applicable to the axial load in column, with $\varepsilon_A = 2 \cdot \varepsilon_{yL} = \varepsilon_{cc\mathrm{MAX}}$, may be defined by Eq. (2.8):

$$f_{cc\mathrm{MAX}} = f_{co} + k_1 \cdot \frac{f_{yL} \cdot A_{sL}}{R \cdot s} \varepsilon_{cc\mathrm{MAX}} = \varepsilon_{co} \cdot (1 + k_3) \tag{2.8}$$

The crucial point in determination of the sectional resistance is definition of the adequate limit state condition. Since the interaction between the concrete column and the transverse spiral reinforcement is a statically indeterminate problem additional equations involving strains must be used. In this work we adopt $\varepsilon_A = 2 \cdot \varepsilon_{sL}$ to link the axial strain and the lateral strain, which is related to the strain in lateral reinforcement. The undertaken assumption allows modification of the standard ACI procedure [29], in which the limit strain in unconfined concrete $\varepsilon_{co} = 0.003$ is used to define the limit state in the cross-section. For eccentric load the assumed limit state condition for a column's section capacity, which is used in further derivations [27], is depicted in Fig. 2. Locations of points G and P in the graph depend on formulae in Eq. 2.5 to Eq. (2.8) and on dimensions of the column's cross-section and material properties of concrete and steel. When confinement effect is activated ($\varepsilon_A > 0$) the maximum strain is larger than for unconfined concrete ($\varepsilon_{cc} > \varepsilon_{co} = 0.003$).

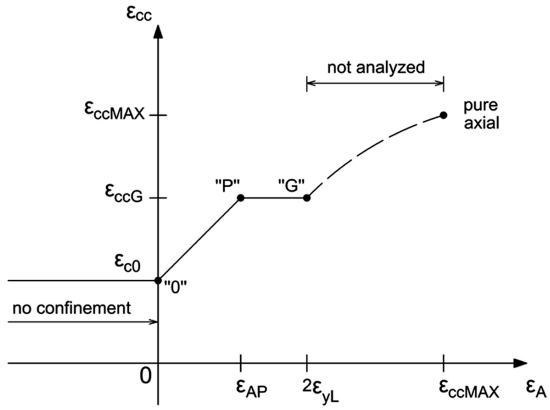

Fig. 2. Adopted limit state strains for confined columns

3. Procedure for calculation of nominal resistance

The calculation procedure for determination of nominal resistance of confined circular concrete columns with spiral transverse reinforcement is developed based on the procedure for unconfined circular columns described by T. Lutomirski [23]. It allows plotting interaction diagrams for combinations of force and moment, including the characteristic points, as shown schematically in Fig. 3 and described below in this chapter.

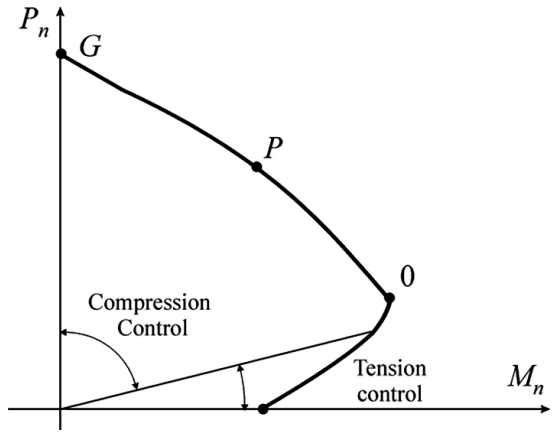

Fig. 3. Interaction diagram with characteristic points

The limit state of a column's cross-section is governed by limit strains $\varepsilon_{cc} > \varepsilon_{co}$ in confined or $\varepsilon_{co} = 0.003$ in unconfined concrete (both under compression control) or tensile limit strain in extreme longitudinal reinforcement strains $\varepsilon_{yu} = 0.005$ (tension control) [22–25]. Because of the material models assumed and dimensions of the circular cross-section several cases must be analysed to obtain complete force-moment interaction diagram.

First, the position of each longitudinal bar D_i is computed with the respect to the referential extreme top fibres of the cross-section, and the location of the lowest reinforcing bar ζ is calculated as the maximum value of such distance using Eq. (3.1). Positioning of bars in the procedure and notation used is visualized in Fig. 4.

$$D_i = R - \cos(\psi + \beta \cdot (i-1)) \cdot \left(R - t - \frac{d}{2}\right)\zeta = \max(D_i) \tag{3.1}$$

where: R – radius of concrete cross-section, ψ – shift angle of the first reinforcement bar, β – angle between the consecutive reinforcement bars, i – number of i^{th} reinforcement bar in cross-section, t – concrete cover, d – diameter of a single reinforcement bar.

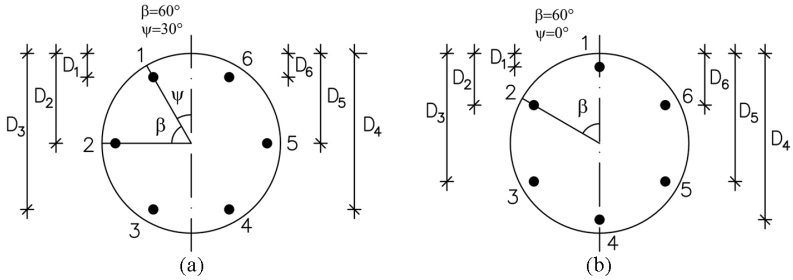

Fig. 4. Description of reinforcing bars positioning for the procedure: (a) $\psi = 30°$, (b) $\psi = 0°$

The depth of the equivalent compressive stress block a is chosen to become a control parameter, which determines the particular ranges of maximum compressive strain in the extreme top fibres of the confined concrete cross-section. The size of the reduced compression block is described by Eq. (3.2) with a reduction factor for the compressive zone in concrete as defined by Eq. (3.3).

$$a = \beta_1 \cdot c \tag{3.2}$$

$$\beta_1 = \begin{cases} 0.85 & \text{for } f_c' \leq 4ksi \\ 1.05 - 0.05 f_c' & \text{for } 4ksi < f_c' < 8ksi \\ 0.65 & \text{for } f_c' \geq 8ksi \end{cases} \tag{3.3}$$

where: β_1 – a reduction factor for the compressive zone in concrete, c – position of the neutral axis, $f_c' = f_{co}$ – compressive strength of unconfined concrete.

3.1. Confinement effect in cross-section

In the following subchapter, the details of the strain control procedure with active confinement effect are presented. The remaining steps of the procedure can be found in [23, 24] for circular columns or [19–22] for rectangular columns.

The first characteristic point G on the interaction diagram, corresponding to the value a_G, is defined by Eq. (3.4). It is assumed that the stress block covers the whole cross-section and

the spiral and extreme longitudinal reinforcement simultaneously reach their yield strains, ε_{yL} and ε_y respectively, as shown in Fig. 5a. It is valid for all values $a \geq a_G$, even if some nonuniform deformation is present, but resistance moment is still null. The proportion equation for the strains in the cross-section based on Fig. 5a allows calculation of the limit strain value ε_{ccG} by Eq. (3.5). It corresponds to the situation when the pure axial capacity of a column cross-section is reached. The obtained value is usually lower than the maximum ductility strain $\varepsilon_{cc\mathrm{MAX}}$ calculated with Richart's formula Eq. (2.8). Therefore, the value $\varepsilon_{cc\mathrm{MAX}}$ is greater than it is needed to reach yield stress in the spiral reinforcement. Thus, both values ε_{ccG} and $\varepsilon_{cc\mathrm{MAX}}$ can be equalized in order to obtain the appropriate amount of spiral reinforcement, so that both the concrete and the lateral spiral reinforcement can be used economically, as described by Eq. (3.6).

$$a_G = \zeta \cdot \frac{\beta_1 \cdot \varepsilon_{ccG}}{\varepsilon_{ccG} - \varepsilon_y} a_G \geq 2R \tag{3.4}$$

$$\varepsilon_{ccG} = \frac{2\varepsilon_{yL} \cdot \zeta - \varepsilon_y \cdot R}{\zeta - R} \tag{3.5}$$

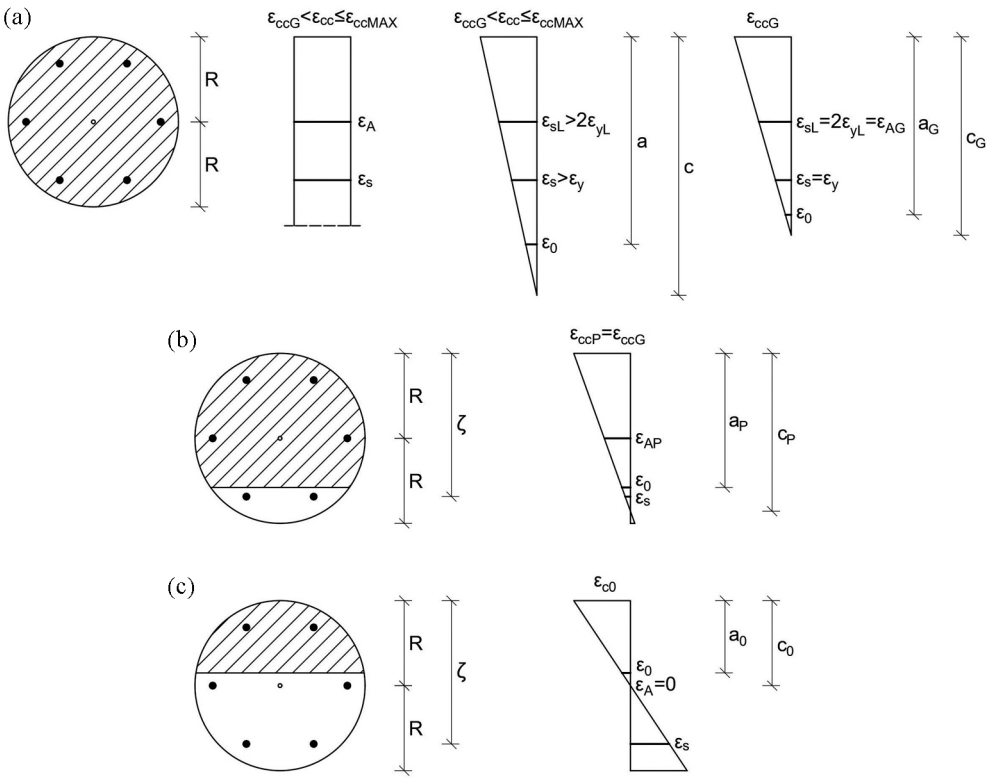

Fig. 5. Distribution of longitudinal strains: (a) for point G (uniform, nonuniform $\infty < a \leq a_G$, and limit case $a = a_G$, $a_G \geq 2R$), (b) for point P, (c) for the point 0

$$\frac{A_{sL}}{R \cdot s} > \frac{f_{co}}{k_2 \cdot f_{yL}} \left(\frac{\varepsilon_{ccG}}{\varepsilon_{co}} - 1 \right) \tag{3.6}$$

The confinement effect, which is the largest for pure axial loading, decreases beyond point G due to the developing bending moment. The next characteristic point P, for which $a_P < a_G$, is defined by the condition that maximum strain in the confined concrete ε_{ccP} is still equal to the previously obtained ε_{ccG} but it reaches the maximum allowed value in Eq. (2.8) for lateral reinforcement in the elastic range. The location of this transition point is calculated using Eq. (2.7). The axial strain value ε_{AP} may be calculated from Richart's formula in Eq. (2.6). Then, the location a_P of the characteristic point P is received from the proportion of strains in the cross-section, as presented in Fig. 5b and described by Eq. (3.7):

$$\varepsilon_{AP} = \frac{2\varepsilon_{yL}}{k_3} \cdot \left(\frac{\varepsilon_{ccG}}{\varepsilon_{c0}} - 1 \right) a_P = \frac{\beta_1 \cdot \varepsilon_{ccG} \cdot R}{\varepsilon_{ccG} - \varepsilon_{AP}} \tag{3.7}$$

The point 0 with location a_0 is the last characteristic point needed in the analysis and represents the end of the confinement effect. From this point $a < a_0$ the maximum strain ε_{co} and the compressive strength f_{co} of concrete are equal to the values for an unconfined column. This condition is valid when the longitudinal strain in the axis of the concrete column is $\varepsilon_A = 0$, which previously implied the effect of the spirals and as a result the increase of compressive strength of concrete f_{cc}. The depth of the compression block that represents the situation at point 0 is defined in Eq. (3.8) and corresponding strength and strain are given by next formulae in Eq. (3.8). Distribution of strains for this state is presented in Fig. 5c.

$$a_0 = \beta_1 \cdot R f_{cc0}(a_0) = f_{co} \varepsilon_{cc0}(a_0) = \varepsilon_{co} \tag{3.8}$$

In the next step of the procedure, we analyse the intermediate situations between the defined characteristic points G, P, 0 and form the set of equations based on Richart's formula and the proportion of strains shown in Fig. 6. From this solution it is possible to define functions $\varepsilon_{cc}(a)$ and $\varepsilon_A(a)$ and consequently $f_{cc}(a)$ which represents the increase of compressive strength of confined concrete depending on the position of the limit state point on the interaction diagram.

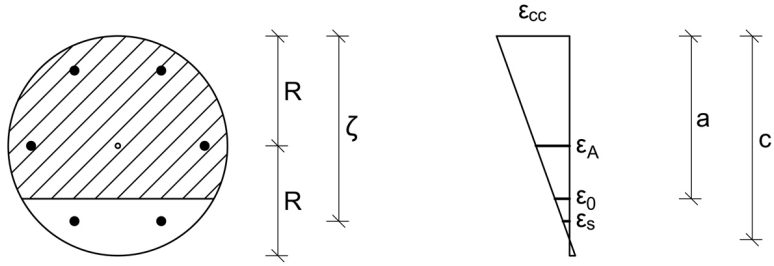

Fig. 6. Distribution of strains depending on size of the compression block a

In the interval $a_P \leq a \leq a_G$ (corresponding to points P and G in Fig. 2 and Fig. 3), the maximum strain in the top fibres of concrete cross-section is defined as $\varepsilon_{cc} = \varepsilon_{ccG}$, while the size of compressive block a and the axial strain $\varepsilon_A(a)$ in concrete column are changing.

Based on the proportion of strains from Fig. 6 the axial strain $\varepsilon_A(a)$ is calculated and then from Richart's formula in Eq. (2.5) the following functions are determined by Eq. (3.9):

$$\varepsilon_{cc}(a) = \varepsilon_{ccG}\varepsilon_A(a) = \varepsilon_{ccG}\left(1 - \beta_1 \cdot \frac{R}{a}\right) f_{cc}(a) = f_{co} + k_1 \cdot \frac{f_{yL} \cdot A_{sL}}{R \cdot s} \cdot \left(\frac{\varepsilon_A(a)}{2\varepsilon_{yL}}\right) \tag{3.9}$$

The functions used in the procedure for the changing parameter a in the range $a_0 < a < a_P$ are described by Eq. (3.10) and Eq. (3.11). They are obtained as the solution of two equations: the proportion of strains from Fig. 7 and Richart's formula in Eq. (2.6), and then using Eq. (2.5).

$$\varepsilon_{cc}(a) = \frac{a \cdot \varepsilon_{co}}{a - (a - \beta_1 \cdot R) \cdot \dfrac{k_3 \cdot \varepsilon_{co}}{2\varepsilon_{yL}}} \varepsilon_A(a) = \frac{(a - \beta_1 \cdot R) \cdot \varepsilon_{co}}{a - (a - \beta_1 \cdot R) \cdot \dfrac{k_3 \cdot \varepsilon_{co}}{2\varepsilon_{yL}}} \tag{3.10}$$

$$f_{cc}(a) = f_{co} + k_1 \cdot \frac{f_{yL} \cdot A_{sL}}{R \cdot s} \cdot \left(\frac{\varepsilon_A(a)}{2\varepsilon_{yL}}\right) \tag{3.11}$$

The confinement effect vanishes when $a \leq a_0$ (or $\varepsilon_A < 0$) and then consequently the procedure for unconfined columns is used [29] with:

$$f_{cc} = f_{co}\, \varepsilon_{cc} = \varepsilon_{co} \tag{3.12}$$

3.2. Calculation of force and moment for interaction diagram

In the procedure [23, 24] for creating the force-moment interaction diagram it is necessary to compute strains for each value of driving parameter a and for each reinforcement bar which can be derived from Eq. (3.13):

$$\varepsilon_s(i, a) = \varepsilon_{cc}(a) \cdot \left(1 - \frac{R - \cos(\psi + \beta(i-1)) \cdot (R - t - \frac{d}{2})}{c(a)}\right) \tag{3.13}$$

Model of steel for longitudinal reinforcement is as in Eq. (3.14):

$$f_s = \begin{cases} f_y & \text{for } \varepsilon_y < \varepsilon_s \leq \varepsilon_{cc} \\ E_s \cdot \varepsilon_s & \text{for } -\varepsilon_y \leq \varepsilon_s \leq \varepsilon_y \\ -f_y & \text{for } -\varepsilon_{yu} \leq \varepsilon_s < -\varepsilon_y \end{cases} \tag{3.14}$$

where: E_s – modulus of elasticity of longitudinal reinforcement, $\varepsilon_L = f_{yL}/E_{yL}$ – strain in longitudinal reinforcement, f_y – yield stress of longitudinal reinforcement.

Then forces for each bar and each size of the compression block, based on Eq. (3.15), are:

$$P(i, a) = \begin{cases} A_s \cdot f_y & \text{for } \varepsilon_y < \varepsilon_s(i, a) \leq \varepsilon_{cc} \\ A_s \cdot E_s \cdot \varepsilon_s(i, a) & \text{for } -\varepsilon_y \leq \varepsilon_s(i, a) \leq \varepsilon_y \\ -A_s \cdot f_y & \text{for } -\varepsilon_{yu} \leq \varepsilon_s(i, a) < -\varepsilon_y \end{cases} \tag{3.15}$$

The sum of forces constitutes the resultant force of the longitudinal reinforcement.

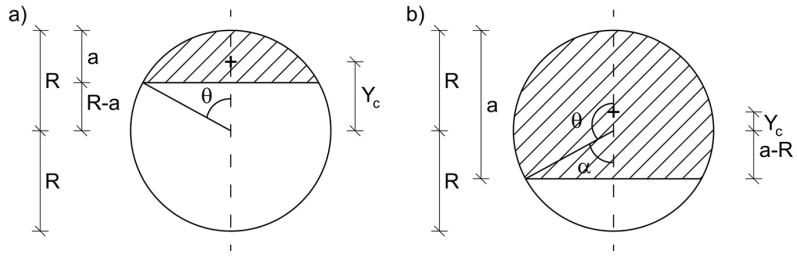

Fig. 7. Description of the size of compressive block in circular concrete

Two cases based on the depth of the compression zone a must be performed for analysis of circular sections in order to obtain the resultant force in concrete, as shown in Fig. 7.

When the depth of the compression zone is smaller than the radius of column $a \leq R$ (Fig. 7a) the half of the acute angle is $\theta \leq 90°$ and derived from Eq. (3.16). If the depth of the compression zone is greater than the radius of column $R < a \leq 2R$ (Fig. 7b) the half of the obtuse angle is $\theta > 90°$ and derived from Eq. (3.17).

$$\theta(a) = \cos^{-1}\left(\frac{R-a}{R}\right) \quad \text{for } a \leq R \tag{3.16}$$

$$\theta(a) = 180 - \alpha(a) \quad \text{and} \quad \alpha(a) = \cos^{-1}\left(\frac{a-R}{R}\right) \quad \text{for } R < a \leq 2R \tag{3.17}$$

The area of the concrete compressive block for a circular column is defined by Eq. (3.18), and the distance of the centroid of the compression block to the section centroid by Eq. (3.19).

$$A(a) = \begin{cases} (2R)^2 \cdot \dfrac{\theta(a) - \sin(\theta(a)) \cdot \cos(\theta(a))}{4} & \text{for } a < 2R \\ \pi \cdot R^2 & \text{for } a \geq 2R \end{cases} \tag{3.18}$$

$$Y_c(a) = \begin{cases} \dfrac{(2R)^3}{A(a)} \dfrac{\sin^3(\theta(a))}{12} & \text{for } \quad a < 2R \\ 0 & \text{for } \quad a \geq 2R \end{cases} \tag{3.19}$$

The concrete stress block resultant force is calculated using Eq. (3.20), while as the total resistance force acting in the cross-section for each size of the compressive block using Eq. (3.21). The total bending moment resistance for each size of the compressive block is expressed by Eq. (3.22).

$$P_c(a) = 0.85 \cdot A(a) \cdot f_{cc}(a) \tag{3.20}$$

$$P_T(a) = \sum_i P(i,a) + P_c(a) \tag{3.21}$$

$$M_T(a) = \sum_i \left[P(i,a) \cdot \cos(\psi + \beta \cdot (i-1)) \cdot \left(R - t - \frac{d}{2}\right)\right] + P_c(a) \cdot Y_c(a) \tag{3.22}$$

3.3. Interaction diagrams for confined and unconfined columns

In order to demonstrate the final result of the procedure presented above, examples of interaction diagrams were plotted and shown in Fig. 8. One design case was selected. The materials and geometry of the circular column and longitudinal reinforcement remain unchanged for unconfined and confined circular concrete columns. For a confined column two cases are considered, with and without concrete cover. The diameter of the concrete column D is equal to 60.96 cm (24 in) with concrete cover equal to 3.81 cm (1.5 in). The compressive strength of concrete f_{co} is 34.5 MPa (5 ksi). The spirals No. 3 with diameter denoted as ϕ_L equal to 0.95 cm (0.375 in) and nominal area A_{sL} = 0.71 cm^2 (0.11 in^2) at 4.06 cm (1.6 in) pitch are assumed. The characteristic yield strength of lateral reinforcement f_{yL} is equal to 414 MPa (60 ksi). The longitudinal reinforcement consists of 12 No. 8 bars (diameter 25.4 mm), Grade 60 and f_y = 414 MPa.

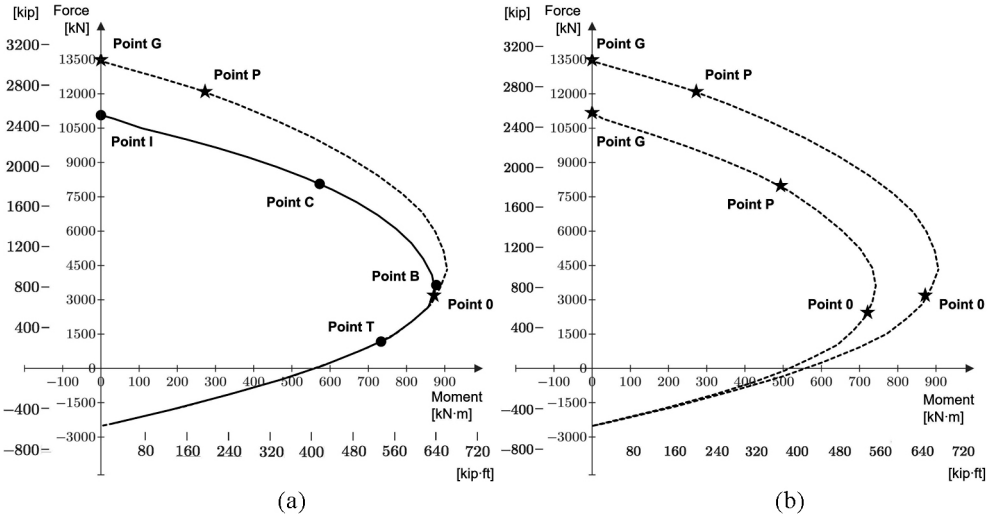

Fig. 8. Examples of interaction diagram: a) for unconfined and confined column with concrete cover, (b) for confined column with and without cover

Comparison of interaction diagrams for unconfined and confined whole column is presented in Fig. 8a. Another comparison of interaction curves for confined column with concrete confined cover included or totally excluded are shown in Fig. 8b. Plotted results allow to qualitatively and quantitatively evaluate the influence of confinement effect. It can be noticed that the contribution of spiral reinforcement in the resistance is significant for the initial part of the diagram, i.e. close to the axial load at point G. The maximum increase of column resistance is 23% for the considered design case (Fig. 8a). Then the effect of confinement smoothly decreases, as it was intended in the proposed model. The more the eccentricity the less the confinement engaged till it vanishes when the axial strain in the concrete column equals zero ($\varepsilon_A = 0$). Presence of $\varepsilon_A > 0$ induces the confinement effect in the column, and $\varepsilon_A < 0$ cancels the confinement thrust. Another comparison of interaction curves for confined column

with concrete cover included or totally excluded are shown in Fig. 8b. The diagram for confined cross-section without concrete cover presents significantly lower resistance due to the ratio of the size of concrete cover to the entire concrete cross-section.

4. Summary and conclusions

The subject of the paper is modelling of the influence of confinement by spiral reinforcement on the resistance of circular concrete columns under eccentric load. The objective is to develop a new procedure that allows calculation and plotting of the force-moment interaction diagrams including the continuously changing effect of confinement. The maximum contribution of spiral reinforcement for the pure axial loading case is based on Richart's model. For increasing eccentricity, the effect of confinement slowly decreases, and then vanishes. To obtain this effect, the strain in spiral reinforcement is related to the axial (uniform vertical) strain in concrete assuming incompressibility of concrete at failure. The stress exerted by the spiral reinforcement induces the increase of concrete resistance due to confinement. When the axial strain in the concrete column reaches zero the effect of confinement on resistance vanishes.

Based on the performed analysis the following conclusions and properties of the presented model can be formulated:

- The procedure is based on similar assumptions for sectional resistance calculations as those included in ACI code and EC2. Thus, it can be conveniently used in design and various structural analyses or research.
- The maximum contribution of spiral reinforcement confinement is for pure axial loading, then with increasing eccentricity the effect of confinement gradually decreases and vanishes for axial strain $\varepsilon_A < 0$.
- The layout of the procedure is quite straightforward, so if needed it can be easily modified to more sophisticated modelling approaches.

References

[1] C.-C. Hou and W.-Z. Zheng, "Review of studies on concrete columns confined by lateral reinforcement under axial compression and lateral cyclic loading", *Structural Concrete*, vol. 24, no. 3, pp. 3592–3619, 2023, doi:10.1002/suco.202200522.

[2] Y.-S. Kim, S.-W. Kim, J.-Y. Lee, J.-M. Lee, H.-G. Kim, and K.-H. Kim, "Prediction of stress-strain behavior of spirally confined concrete considering lateral expansion", *Construction and Building Materials*, vol. 102, pp. 743–761, 2016, doi:10.1016/j.conbuildmat.2015.11.017.

[3] A. Considére, *Resistance a'la compression du ebton arme et du beton frette.* Paris, France: Le Genie Civil, 1903.

[4] F. E. Richart, A. Brandzaeg, and R. L Brown, "A study on the failure of concrete under combine compressive stress", *University of Illinois Bulletin, Engineering Experimental Station*, vol. 185, 1928.

[5] A. Kuryłło, "Nowe doświadczenia ze słupami uzwojonymi", *Inżynieria i Budownictwo*, no. 11, 1952.

[6] H. Rüsch and S. Stöckl, "Versuche an wendelbewehrten Stahlbetonsäulen unter kurz und langzeitig wirkenden zentrischen Lasten", *Deutscher Ausschuss für Stahlbeton*, vol. 205, 1969.

[7] S. Stöckl and B. Menne, "Versuche an wendelbewehrten Stahlbetonsäulen unter exzentrischer Belastung", *Deutscher Ausschuss für Stahlbeton*, vol. 251, pp. 1–66, 1975.

[8] A.B. Nowakowski, "Badania piaskobetonowych słupów uzwojonych pod obciążeniem doraźnym", *Inżynieria i Budownictwo*, no. 8, 1986.

[9] T. Godycki-Ćwirko, P. Korzeniowski, and K. Nagrodzka-Godycka, "O skuteczności uzwojenia w słupach żelbetowych", *Inżynieria i Budownictwo*, no. 12, 1999.

[10] P. Korzeniowski, *Żelbetowe słupy uzwojone: badania i teoria.* Wydawnictwo Politechniki Gdańskiej, 2000.

[11] B. Grzeszykowski and E.D. Szmigiera, " Experimental investigation on the vertical ductility of rectangular CFST columns loaded axially", *Materials*, vol. 15, no. 6, pp. 1–26, 2022 doi:10.3390/ma15062231.

[12] C. Zhou, Z. Chen, Z. Huang, and L. Cai, "Behavior of reinforced concrete columns with double spirals under axial and eccentric loads", *Journal of Building Engineering*, vol. 51, art. no. 104280, 2022, doi:10.1016/j.jobe.2022.104280.

[13] W. Chang and W.-Z. Zheng, "Lateral response of HPC confined by both spiral stirrups and CFRP under axial compression", *Materials and Structures*, vol. 54, art. no. 81, 2021 doi:10.1617/s11527-021-01629-6.

[14] A.S. Sheikh and M.T. Toklucu, "Reinforced concrete columns confined by circular spirals and hoops", *Journal of the American Concrete Institute,* vol. 90-S56, pp. 542–553, 1993.

[15] J.-J. Zeng, Y.-Y. Ye, and W.-T. Liu, "Behaviour of FRP spiral-confined concrete and contribution of FRP longitudinal bars in FRP-RC columns under axial compression", *Engineering Structures*, vol. 281, no. 4, 2023, doi: 10.1016/j.engstruct.2023.115747.

[16] M. Wydra, M. Włodarczyk, and J. Fangrat, "Nonlinear analysis of compressed concrete elements reinforced with FRP bars", *Materials*, vol. 13, no. 19, pp. 1–16, 2020, doi:10.3390/ma13194410.

[17] R. Suhail, G. Amato, and D.P. McCrum, "Active and passive confinement of shape modified low strength concrete columns using SMA and FRP systems", *Composite Structures*, vol. 251, art. no. 112649, 2020, doi:10.1016/j.compstruct.2020.112649.

[18] E.K.Z. Balanji, M.N. Sheikh, and M.N.S. Hadi, "Behaviour of high strength concrete columns reinforced with steel fibres under different eccentric loads", *ACI Structural Journal*, vol. 114, no. 4, 2017, doi:10.14359/51689781.

[19] M.M. Szerszen, A.S. Nowak, and A. Szwed, "Reliability-based resistance of eccentrically loaded columns", in *US- Poland Workshop on Diagnosis of Concrete Materials and Structures for Infrastructure Facilities*. Warsaw, 2004, pp. 145–150.

[20] M.M. Szerszen, A.S. Nowak, and A. Szwed, "Reliability-based sensitivity analysis of RC columns resistance", presented at 9th International Conference on Structural Safety and Reliability, ICOSSAR 2005, Rome, 2005.

[21] A. Szwed, M. M. Szerszeń, and A.S. Nowak, "Wyznaczenie współczynników nośności do projektowania słupów mimośrodowo ściskanych według amerykańskiej normy ACI 318", in *Pięćdziesiąta Jubileuszowa Konferencja Naukowa KILiW PAN KN PZITB*, vol. 3. Krynica, 2004, pp. 83–90.

[22] M.M. Szerszen, A. Szwed, and A.S. Nowak, "Reliability analysis for eccentrically loaded columns", *ACI Structural Journal*, vol. 102, no. 5, pp. 676–688, 2005.

[23] T. Lutomirski, "Reliability models for circular concrete columns", PhD dissertation, University of Nebraska, Lincoln, USA, 2009.

[24] T.A. Lutomirski and M. Lutomirska, "Variability of statistical parameters of resistance for reinforced concrete columns with circular cross-section", *Achieves of Civil Engineering*, vol. 67, no. 2, pp. 165–180, 2021 doi:10.24425/ace.2021.137161.

[25] T.A. Lutomirski and M. Lutomirska, "Strength reduction factor for circular reinforced concrete columns", *ACI Structural Journal*, vol. 119, no. 4, pp. 303–310, 2022, doi:10.14359/51734653.

[26] M. Lutomirska and Sz. Lutomirski, "Cracks in circular reinforced concrete columns occurring during the construction process", *Procedia Engineering*, vol. 153, pp. 419–426, 2016, doi:10.1016/j.proeng.2016.08.144.

[27] A. Łuszczyńska, "Resistance of unconfined and confined circular reinforced concrete columns according to ACI", M.A. thesis, Warsaw University of Technology, 2023.

[28] J.B. Mander, M.J. Priestley, and R. Park, "Theoretical stress-strain model for confined concrete", *ASCE Journal of Structural Engineering*, vol. 114, no. 8, pp. 1804–1826, 1988.

[29] ACI 318-19 Building Code Requirements for Structural Concrete. Farmington Hills, Michigan: American Concrete Institute, 2019.

[30] PN-EN-1992-1-1:2008 Eurocode 2 – Design of concrete structures – Part 1–1: General rules and rules for buildings.

[31] A.M. Abd El Fattah, "Behavior of concrete columns under various confinement effects", PhD dissertation, Kansas State University, 2012.

Model nośności okrągłych skrępowanych słupów żelbetowych pod wpływem obciążeń mimośrodowych

Słowa kluczowe: model nośności, skrępowanie, słupy okrągłe, słupy uzwojone, wykresy interakcji, żelbet

Streszczenie:

Uzwojone słupy żelbetowe, dzięki efektowi skrępowania betonu, wykazują zwiększoną nośność oraz poprawę własności plastycznych. Ich zdolność do znacznych odkształceń przed osiągnięciem nośności jest szczególnie ważna na terenach sejsmicznych. Korzystny wpływ skrępowania po raz pierwszy zostałopisany przez A. Considére ponad 100 lat temu. Kolejne badania w tej dziedzinie dotyczyły między innymi wpływu ilości uzwojenia, klasy betonu, czasu przyłożenia obciążenia, stosowania zbrojenia niemetalicznego czy nowych modeli nośności. Zdecydowana większość badań, zarówno teoretycznych i eksperymentalnych, koncentruje się na ściskaniu osiowym. Badania uwzględniające różne wartości mimośrodu należą do rzadkich. Celem niniejszego artykułu jest zaprezentowanie opracowanego modelu obliczeniowego nośności przekroju skrępowanych słupów o przekroju kołowym z uwzględnieniem rosnącego mimośrodu, umożliwiającego wygenerowanie wykresów interakcji siły i momentu zginającego. W przedstawionym modelu maksymalne naprężenia i odkształcenia dla betonu skrępowanego, odpowiadające przypadkowi osiowego ściskania, obliczane są na podstawie modelu Richarta. Następnie, wpływ skrępowania na nośność słupa zostaje uzależniony od odkształceń w osi słupa ε_A. Dzięki temu spada on wraz ze wzrostem mimośrodu i zanika dla odkształceń w osi słupa równych zero. Wówczas początkowo znaczna wytrzymałość na ściskanie betonu skrępowanego f_{cc} i odpowiadające jej odkształcenie ε_{cc} osiągają wartości jak dla betonu nieskrępowanego f_{co} i ε_{co}. Podstawą opracowanego modelu są założenia prostokątnego rozkładu naprężeń ściskających w betonie, zgodności odkształceń oraz idealnej przyczepności między zbrojeniem a betonem, linowo sprężysta, a następnie idealnie plastyczna zależność pomiędzy naprężeniami a odkształceniami dla zbrojenia podłużnego, oraz sprężysto-plastyczna dla zbrojenia spiralnego przy rozciąganiu. Odkształcenie poprzeczne betonu skrępowanego jest trudne do dokładnego oszacowania. Przy wzrastającym obciążeniu, początkowo wartość współczynnika Poisson dla betonu pozostaje stała i wynosi 0.2. Przy wartości naprężenia równej w przybliżeniu $0.8 f_{co}$, zaczyna ona gwałtownie rosnąć do wartości odpowiadającej materiałowi nieściśliwemu, czyli 0.5. W związku z powyższym, dla potrzeb modelu, odkształcenie w zbrojeniu spiralnym ε_{sL} przyjęto równe połowie osiowego odkształcenia w słupie ε_A. Przedstawiona procedura generowania wykresów interakcji umożliwia uwzględnienie różnych średnic słupów, wytrzymałości betonu na ściskanie, granicy plastyczności stali, modułu sprężystości stali, ilości prętów, ich rozmiarów i położenia. Zmienność mimośrodu siły definiowana jest poprzez zmianę wielkości strefy ściskanej betonu a. Procedura dla słupów okrągłych bez uwzględnienia skrępowania została opublikowana przez T. Lutomirskiego. Stan graniczny nośności definiowany jest przez osiągnięcie odkształceń granicznych, w betonie skrępowanym $\varepsilon_{cc} > \varepsilon_{co}$, oraz w betonie nieskrępowanym $\varepsilon_{co} = 0.003$. Wprowadzono nowe punkty charakterystyczne. Pierwszy, nazwany punktem G, odpowiada sytuacji, w której cały przekrój jest ściskany ($a_G \geq 2R$) a odkształcenia w zbrojeniu podłużnym i porzecznym osiągają jednocześnie wartości graniczne, ε_{yL} i ε_y. Z proporcji odkształceń wyprowadzone zostaje odkształcenie graniczne betonu skrępowanego ε_{ccG}, które jest mniejsze od maksymalnego odkształcenia plastycznego $\varepsilon_{cc\mathrm{MAX}}$ z formuły Richarta. Zatem wartość $\varepsilon_{cc\mathrm{MAX}}$ jest większa od wartości koniecznej do uplastycznienia zbrojenia spiralnego. Przyrównując te dwa odkształcenia, można otrzymać optymalną ilość zbrojenia spiralnego. Kolejnym punktem charakterystycznym jest przejściowy punkt P, $a_P < a_G$, dla którego odkształcenie ε_{ccP} jest równe ε_{ccG}, które osiąga wartość maksymalną $\varepsilon_{cc\mathrm{MAX}}$ przewidywaną w modelu Richarta. Odkształcenie

w osi słupa ε_{AP} obliczane jest na podstawie formuły Richarta. Następnie z proporcji obliczana jest wielkość ściskanego bloku betonowego a_P. Punkt 0 odpowiada końcowi wpływu skrępowania. Odkształcenia w osi słupa ε_A osiągają wówczas wartość zero. Dla ściskanego bloku betonowego o $a<a_0$, maksymalne odkształcenie i wytrzymałość betonu na ściskanie równe są wartościom dla elementów nieskrępowanych, czyli odpowiednio ε_{co} i f_{co}. Dla sytuacji pośrednich, pomiędzy punktami charakterystycznymi, zdefiniowano funkcje $\varepsilon_{cc}(a)$, $\varepsilon_A(a)$ oraz $f_{cc}(a)$, zależne od zmniejszającego się ściskanego bloku betonowego umożliwiające uwzględnienie zanikającego wpływu skrępowania. Następnie możliwe jest obliczenie wszystkich wartości siłi momentów zginających tworzących wykres interakcji. Efekt działania opracowanego modelu i procedury obliczeniowej, zostałzwizualizowany na podstawie jednego wybranego przypadku obliczeniowego. W celach porównawczych wygenerowano dwa wykresy, dla słupa o przekroju kołowym z uwzględnieniem skrępowania i bez. Dla słupa skrępowanego ściskanego osiowo otrzymano nośność o 23% większą niż dla nieskrępowanego. Następnie widoczny jest stopniowy zanik wpływu skrępowania, aż do jego całkowitego braku, co jest zgodne z zamierzeniami autorów. Zaprezentowano wyniki obliczeń zarówno dla modelu uwzględniającego otulinę jak również jej brak wnioskując, że różnica między nimi może być znaczna i jest zależna od geometrii przekroju.

Received: 2023-12-22, Revised: 2024-03-26